Supplementary Information (SI)

Photophysical Studies of low symmetry Sm(III) and Tb(III) complexes reveal remarkable quantum yields

Asgar Ali,*[1] Zubair Ahmed,*[2] Khalid Iftikhar[1] and Rahisuddin*[1]

[1]Lanthanide Research Laboratory, Department of Chemistry, Jamia Millia Islamia, New Delhi 110025, India.
[2] School of Chemical Sciences, Universiti Sains Malaysia, Gelugor 11800, Pulau Pinang, Malaysia.
E-mails for correspondence: asgar.chemistry@gmail.com, rahisuddin@jmi.ac.in

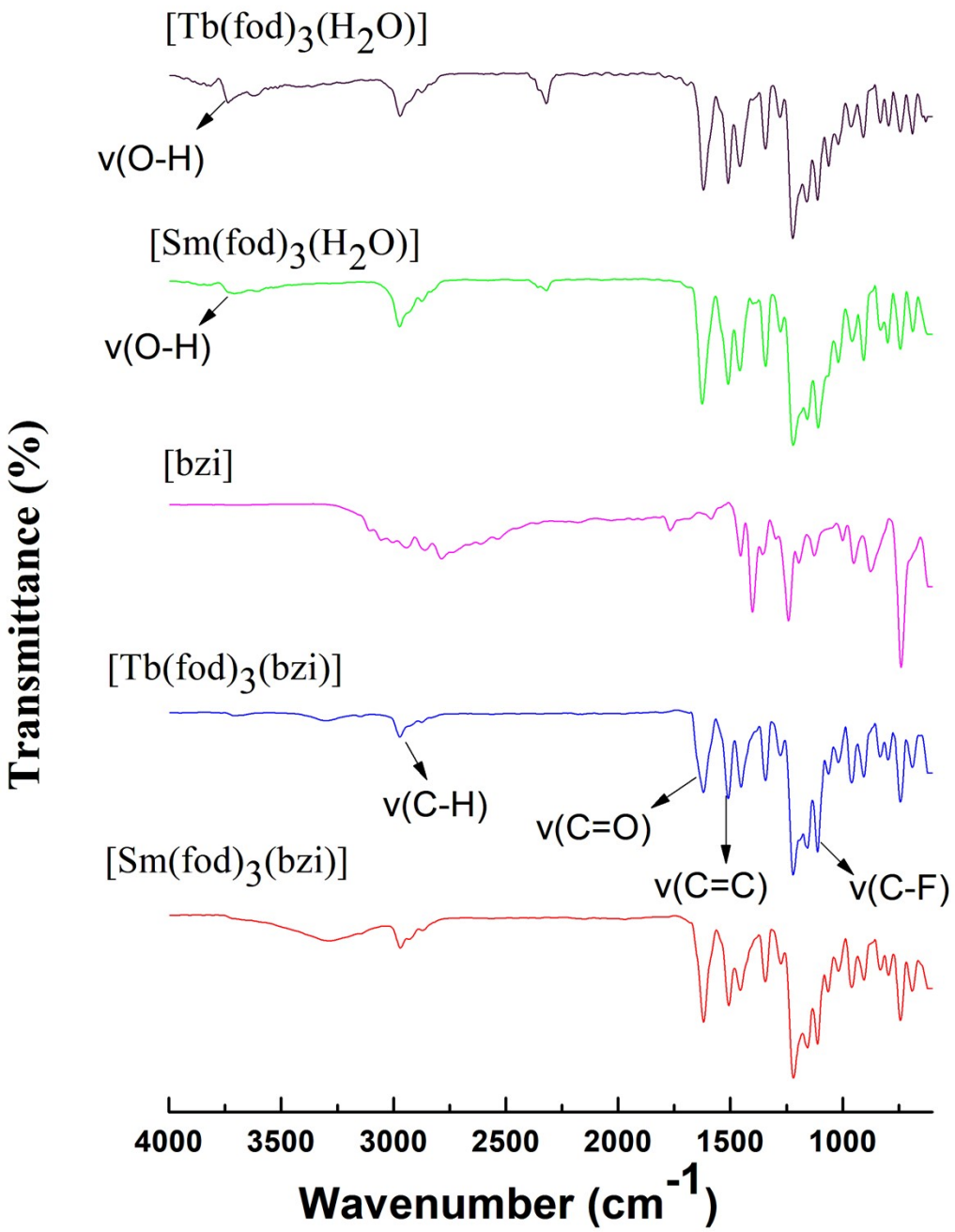

Figure S1. FTIR spectra of ligand and complexes.

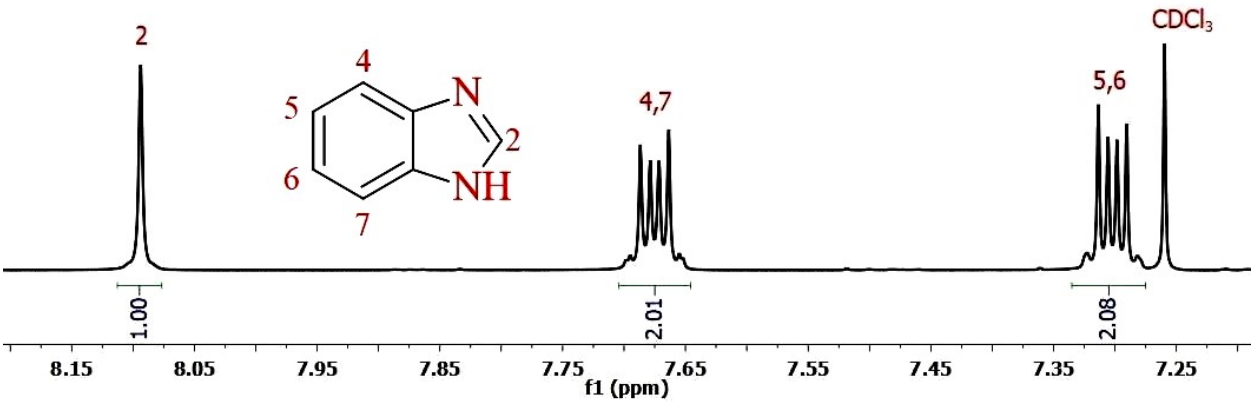

Figure S2. 500 MHz ^{1}H NMR spectra of benzimidazole in $CDCl_3$.

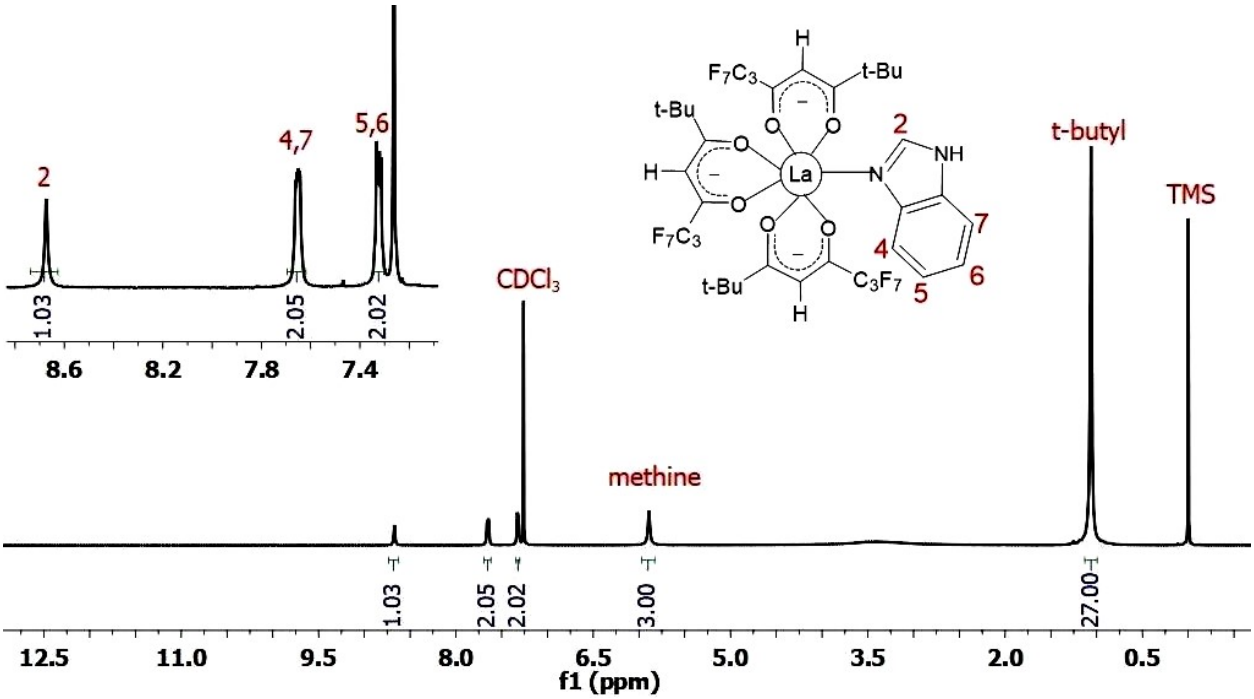

Figure S3. 500 MHz ^{1}H NMR spectra of $[La(fod)_3(terpy)]$ in $CDCl_3$.

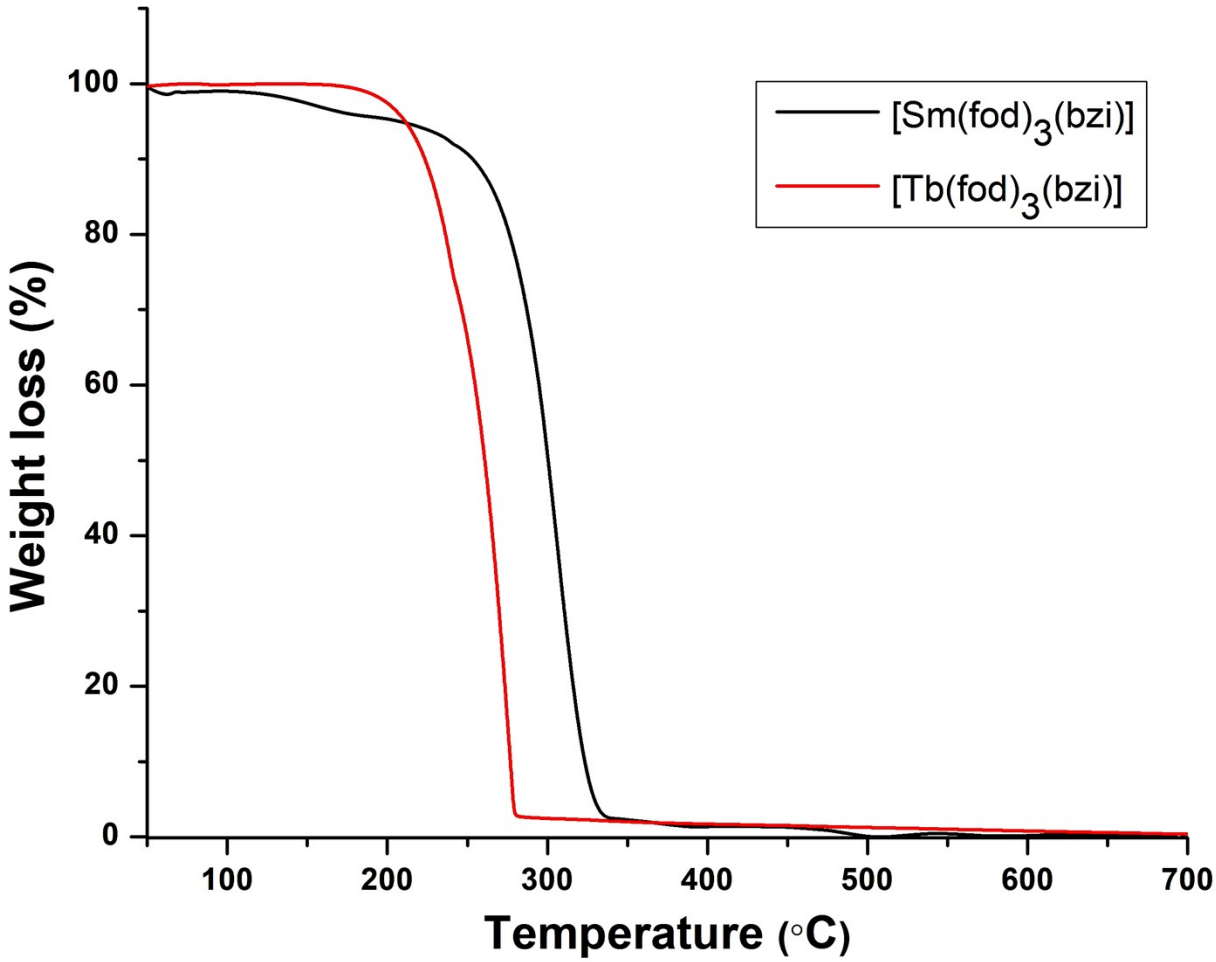

Figure S4. TGA of the complexes.

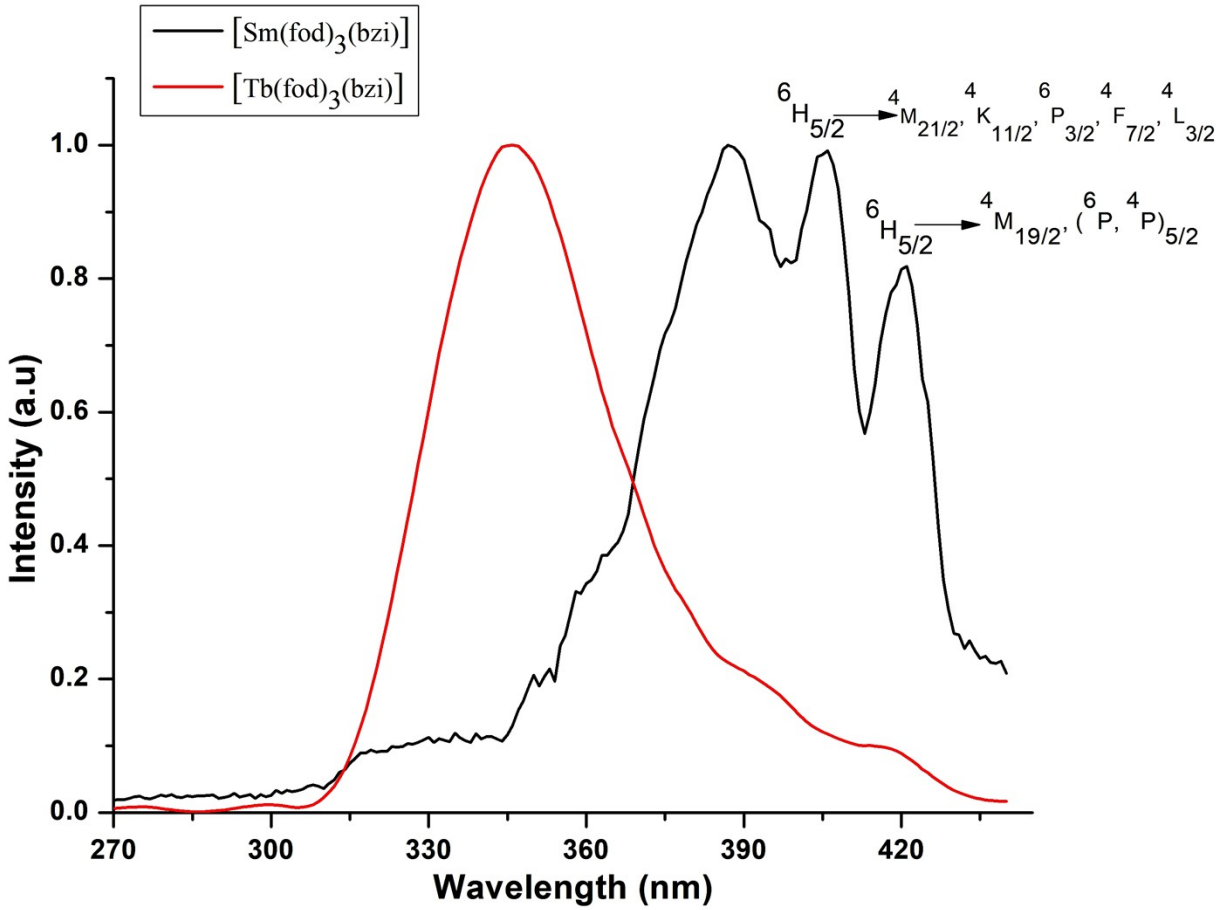

Figure S5. Excitation spectra of complexes in solid state.

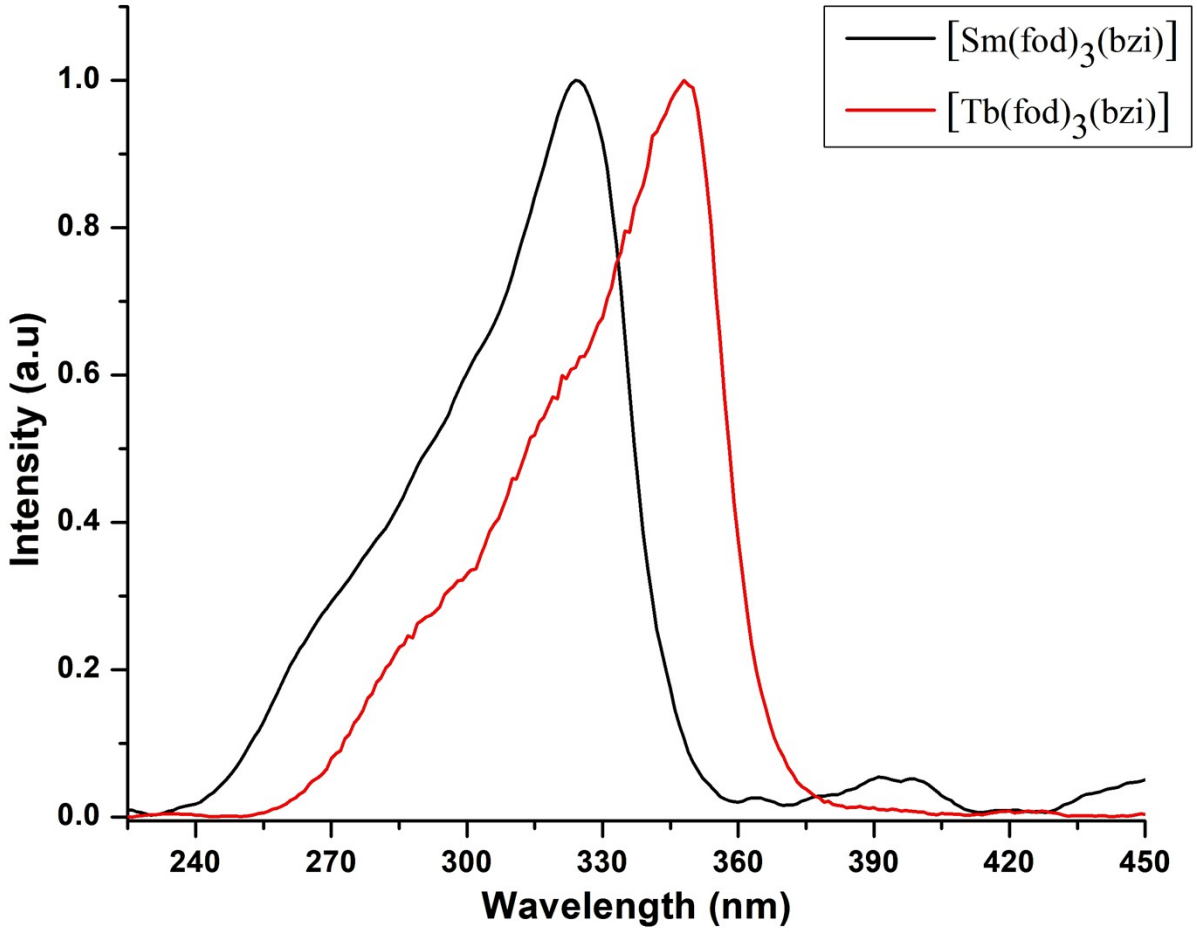

Figure S6. Excitation spectra of complexes in 3% PMMA thin film.

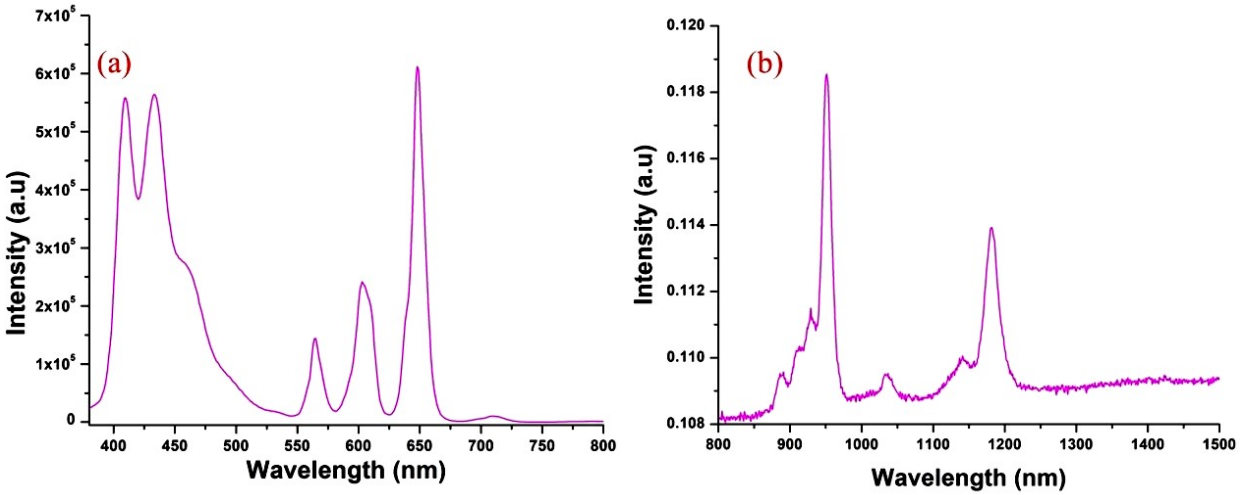

Figure S7. (a) Visible and (b) Near infra-red emission spectra of $[Sm(fod)_3(H_2O)]$ in chloroform

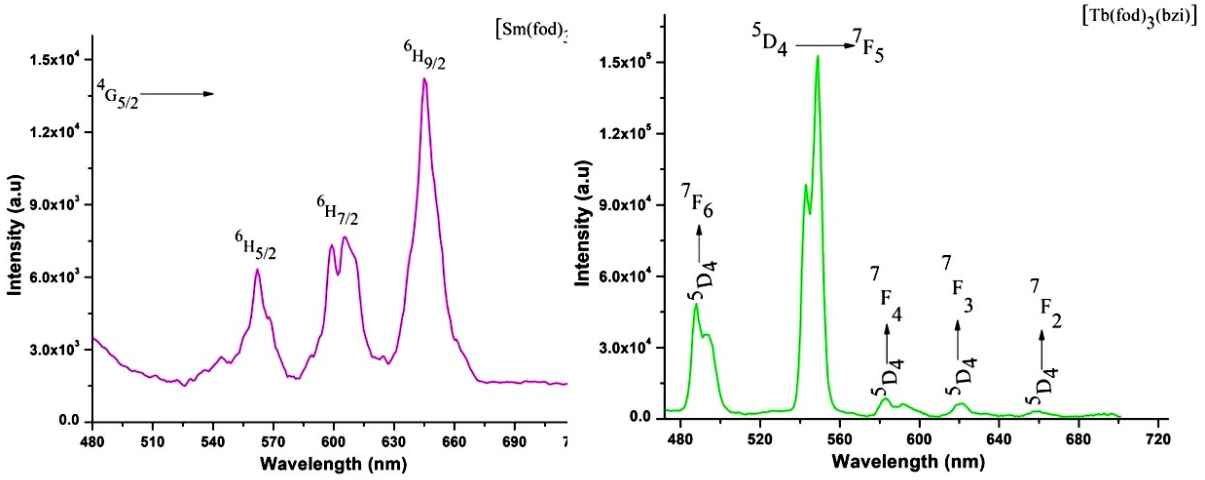

Figure S8. Emission spectra of complexes in solid state.

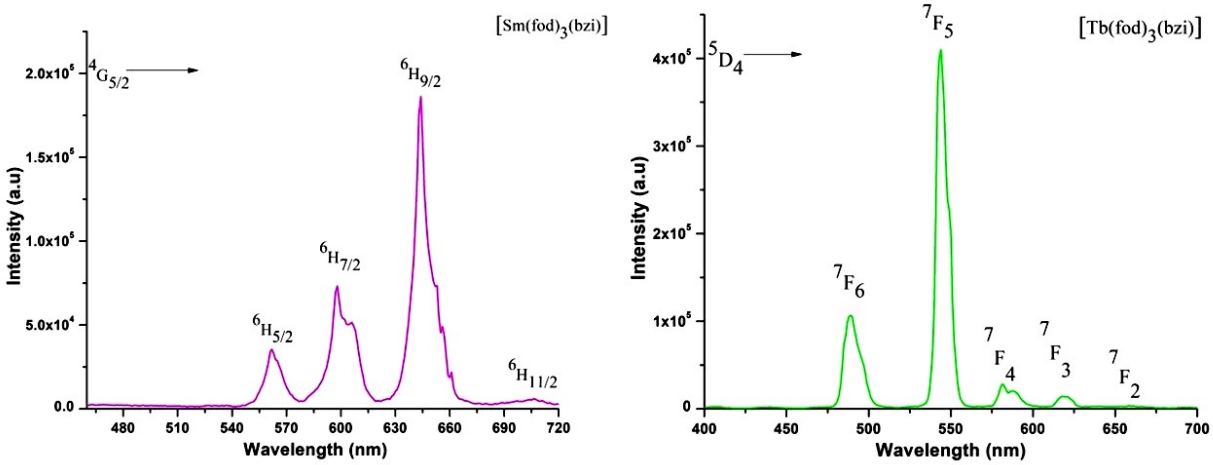

Figure S9. Emission spectra of complexes in 3% PMMA thin film.

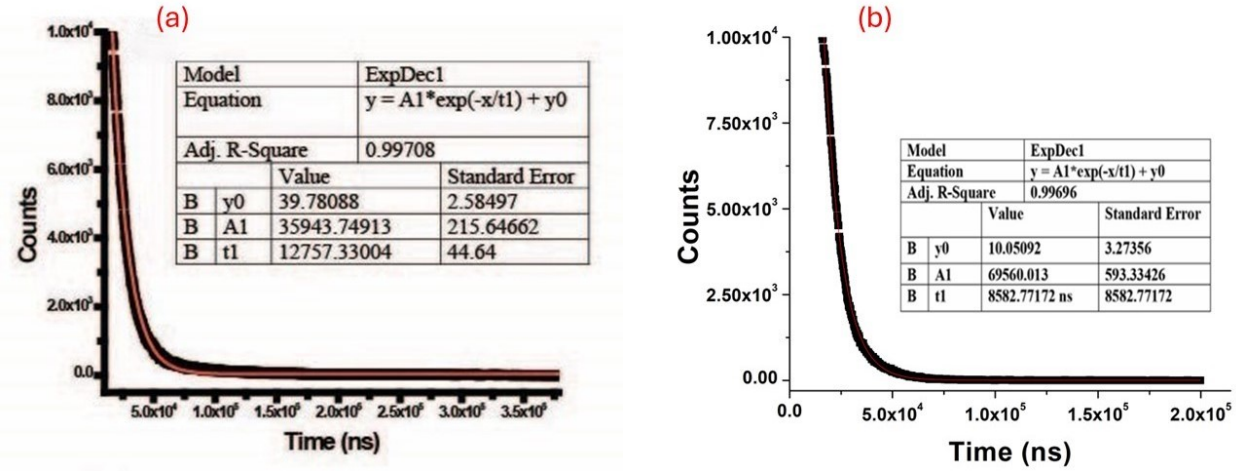

Figure S10. Emission decay profile of (a) complex **1** and (b) complex **2** in chloroform (λ_{max} = 343 (Sm^{III}) and 33 (Tb^{III}) nm and $c = 5\times10^{-5}$M).

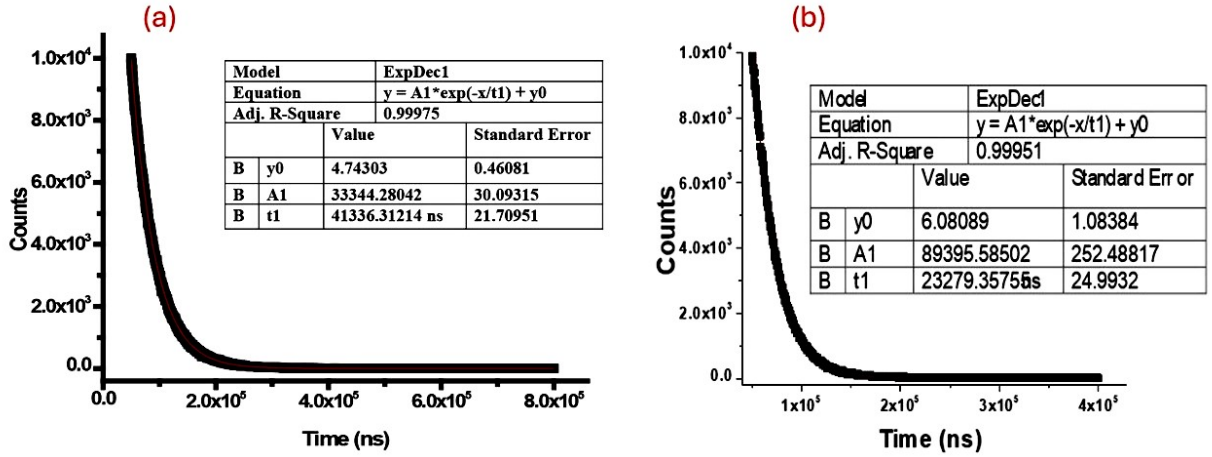

Figure S11. Emission decay profile of (a) [Sm(fod)$_3$(bzi)] (1), and (b) [Tb(fod)$_3$(bzi)] (2) in solid state.

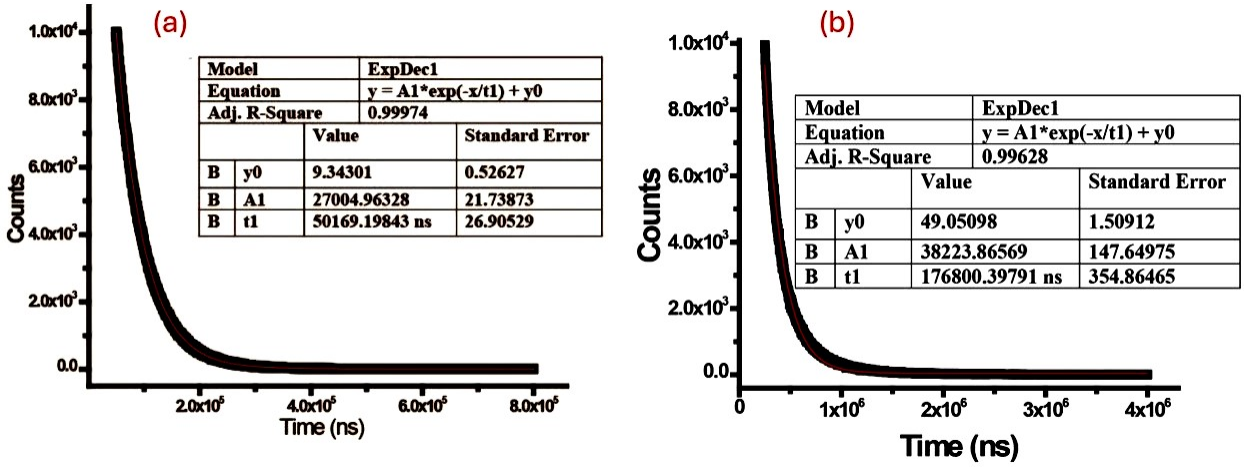

Figure S12. Emission decay profile of (a) [Sm(fod)$_3$(bzi)] (1), and (b) [Tb(fod)$_3$(bzi)] (1) in 3% PMMA thin film.

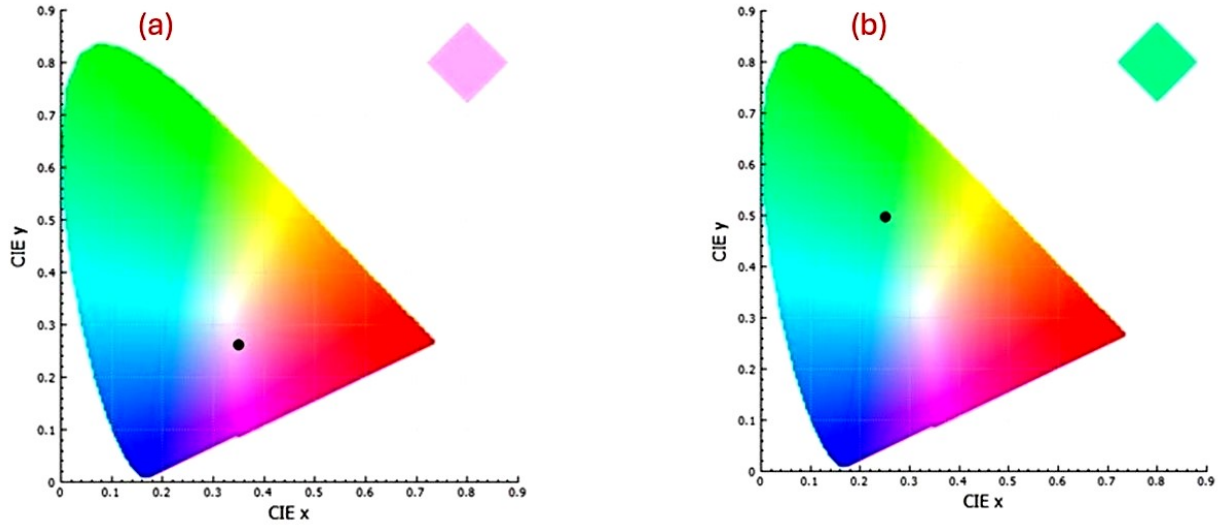

Figure S13. CIE chromaticity diagram of (a) [Sm(fod)$_3$(bzi)] (1), and (b) [Tb(fod)$_3$(bath)] (2), in solid state.

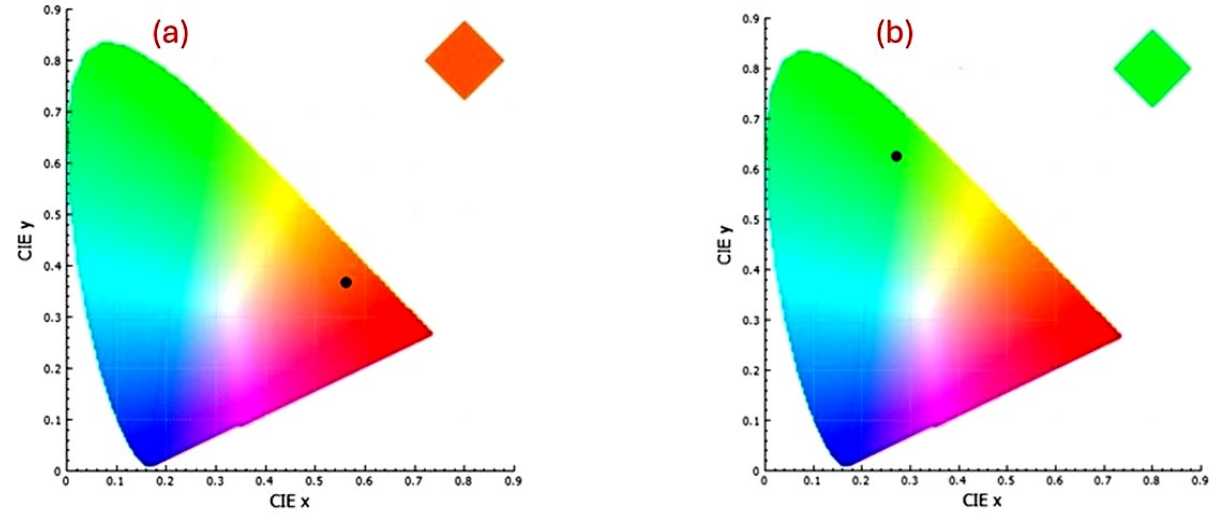

Figure S14. CIE chromaticity diagram of (a) [Sm(fod)$_3$(bzi)] (1), and (b) [Tb(fod)$_3$(bath)] (2), in 3% PMMA thin film.

Table S1. Selected bond lengths (Å) and bond angles (˚) of [Tb(fod)$_3$(bzi)] (2)

Tb(1)-O(3)	2.354(4)	O(3)-Tb(1)-O(4)	74.27(13)	O(4)-Tb(1)-O(2)	79.98(15)
Tb(1)-O(4)	2.332(4)	O(3)-Tb(1)-O(6)	83.86(14)	O(6)-Tb(1)-O(2)	85.24(16)
Tb(1)-O(6)	2.315(4)	O(4)-Tb(1)-O(6)	78.42(16)	O(5)-Tb(1)-O(2)	79.13(16)

Tb(1)-O(5)	2.292(4)	O(3)-Tb(1)-O(5)	120.08(15)	O(3)-Tb(1)-O(1)	105.86(15)
Tb(1)-O(2)	2.304(4)	O(4)-Tb(1)-O(5)	145.70(14)	O(4)-Tb(1)-O(1)	77.62(15)
Tb(1)-O(1)	2.277(4)	O(6)-Tb(1)-O(5)	73.01(15)	O(6)-Tb(1)-O(1)	150.43(16)
Tb(1)-N(1)	2.472(5)	O(3)-Tb(1)-O(2)	153.56(16)	O(5)-Tb(1)-O(1)	121.38(15)
O(2)-Tb(1)-O(1)	73.75(16)	O(3)-Tb(1)-N(1)	80.60(14)	O(4)-Tb(1)-N(1)	138.69(15)
O(6)-Tb(1)-N(1)	131.08(16)	O(5)-Tb(1)-N(1)	75.54(14)	O(2)-Tb(1)-N(1)	124.05(16)
O(1)-Tb(1)-N(1)	78.45(15)				

Table S2. SHAPE measured deviations from ideal seven coordinate geometries of [Tb(fod)$_3$(bzi)] (2) complex.

S. No.	SHAPE	Symmetry	Deviation
1	Heptagon	D_{7h}	34.960
2	Hexagonal pyramid	C_{6v}	19.781
3	Pentagonal bipyramid	D_{5h}	6.743
4	Capped octahedron	C_{3v}	**0.637**
5	Capped trigonal prism	C_{2v}	1.015
6	Johnson pentagonal bipyramid J13	D_{5h}	10.223
7	Johnson elongated triangular pyramid J7	C_{3v}	18.158

Table S3. SHAPE measured deviations from ideal seven coordinate geometry in Sparkle/PM7 predicted [Sm(fod)$_3$(bzi)] (1) and [Tb(fod)$_3$(bzi)] (1) complex.

S. No.	SHAPE	Symmetry	Deviation [Sm(fod)$_3$(bzi)] (1)	Deviation [Tb(fod)$_3$(bzi)] (2)
1	Heptagon	D_{7h}	33.519	31.461
2	Hexagonal pyramid	C_{6v}	17.137	21.481
3	Pentagonal bipyramid	D_{5h}	8.934	7.160
4	Capped octahedron	C_{3v}	**2.442**	3.134
5	Capped trigonal prism	C_{2v}	3.416	**2.306**
6	Johnson pentagonal bipyramid J13	D_{5h}	12.945	10.493
7	Johnson elongated triangular pyramid J7	C_{3v}	20.511	16.254